Seasonal Variation of the Physical Properties of Marine Boundary Layer Clouds off the California Coast

WUYIN LIN AND MINGHUA ZHANG

School of Marine and Atmospheric Sciences, Stony Brook University, Stony Brook, New York

NORMAN G. LOEB

NASA Langley Research Center, Hampton University, Hampton, Virginia

(Manuscript received 13 February 2008, in final form 12 August 2008)

ABSTRACT

Marine boundary layer (MBL) clouds can significantly regulate the sensitivity of climate models, yet they are currently poorly simulated. This study aims to characterize the seasonal variations of physical properties of these clouds and their associated processes by using multisatellite data. Measurements from several independent satellite datasets [International Satellite Cloud Climatology Project (ISCCP), Clouds and the Earth's Radiant Energy System–Moderate Resolution Imaging Spectroradiometer (CERES–MODIS), Geoscience Laser Altimeter System (GLAS), and Cloud-Aerosol Lidar and Infrared Pathfinder Satellite Observation (CALIPSO)], in conjunction with balloon soundings from the mobile facility of the Atmospheric Radiation Measurement (ARM) program at Point Reyes and reanalysis products, are used to characterize the seasonal variations of MBL cloud-top and cloud-base heights, cloud thickness, the degree of decoupling between clouds and MBL, and inversion strength off the California coast.

The main results from this study are as follows: (i) MBL clouds over the northeast subtropical Pacific in the summer are more prevalent and associated with a larger in-cloud water path than in winter. The cloud-top and cloud-base heights are lower in the summer than in the winter. (ii) Although the lower-tropospheric stability of the atmosphere is higher in the summer, the MBL inversion strength is only weakly stronger in the summer because of a negative feedback from the cloud-top altitude. Summertime MBL clouds are more homogeneous and are associated with lower surface latent heat flux than those in the winter. (iii) Seasonal variations of low-cloud properties from summer to winter resemble the downstream stratocumulus-to-cumulus transition of MBL clouds in terms of MBL depth, cloud-top and cloud-base heights, inversion strength, and spatial homogeneity. The ''deepening–warming'' mechanism of Bretherton and Wyant for the stratocumulus-to-trade-cumulus transition downstream of the cold eastern ocean can also explain the seasonal variation of low clouds from the summer to the winter, except that warming of the sea surface temperature needs to be taken as relative to the free-tropospheric air temperature, which occurs in the winter. The observed variation of low clouds from summer to winter is attributed to the much larger seasonal cooling of the free-tropospheric air temperature than that of the sea surface temperature.

1. Introduction

Marine boundary layer (MBL) clouds play a vital role in the earth's climate system because of their abundance and strong net radiative cooling effect (see, e.g., Klein and Hartmann 1993). They have been identified in the Intergovernmental Panel on Climate Change's (IPCC's) fourth assessment (Randall et al. 2007) as a primary source of uncertainty in determining the sensitivity of climate models. The difficulty of accurately modeling MBL clouds results from the highly interactive nature of these clouds with the turbulent boundary layer and the subtle balances among the governing processes of turbulence, microphysics, and radiation. Theoretical studies have been designed to tackle these balances for the maintenance of MBL clouds (e.g., Lilly 1968; Nicholls 1984; Turton and Nicholls 1987) and their evolutions in the transitional zone (e.g., Randall 1980; Krueger et al. 1995; Bretherton and Wyant 1997). Such studies and

Corresponding author address: Dr. Wuyin Lin, School of Marine and Atmospheric Sciences, Stony Brook University, Stony Brook, NY 11794.
E-mail: wlin@atmsci.msrc.sunysb.edu

DOI: 10.1175/2008JCLI2478.1

several MBL field experiments (e.g., Albrecht et al. 1988, 1995; Stevens et al. 2003; Bretherton et al. 2004) have largely targeted the spatial evolution of MBL clouds from stratocumulus to cumulus, in particular for the northern summer when MBL and clouds are stable and well defined.

A few studies have also examined the seasonal variations of MBL clouds using surface-based (e.g., Klein and Hartmann 1993) and spaceborne (e.g., Rozendaal and Rossow 2003) datasets. These studies have focused on the cloud amount over the eastern oceans. Klein and Hartmann (1993) described the influence of large-scale environment on the amount of MBL clouds and showed a very good correlation between monthly cloud amount and lower-tropospheric stability (LTS) of the atmosphere. Few studies have investigated the seasonal variations of the MBL structure and the associated physical properties of clouds besides cloud amount, although they are much needed for the understanding of cloud processes and as a natural test of climate models.

MBL clouds are generally situated just below the inversion base. The cloud-top temperature derived from spaceborne radiance is therefore a good measure of the air temperature at the inversion base. Before active sensors of clouds became available, cloud-top temperature has been used to infer cloud-top pressure and thus height, which are known to be biased over MBL with temperature inversions. Active sensors from spaceborne lidar provide direct measurements of cloud-top height. The temporal and spatial sampling from these sensors, however, is relatively poor. We therefore use data from both passive and active sensors to study the seasonal variation of cloud top.

To translate the cloud-top temperature from passive sensors to the cloud-top height, a priori knowledge of atmospheric temperature profile (usually from operational analysis; e.g., Menzel et al. 2006) is required. The operational analysis is often not suited for this purpose because the MBL structure strongly depends on the physical processes that cannot be satisfactorily resolved by models used for the analysis. Several studies have used the MBL temperature lapse rate to derive the cloud-top height from cloud-top temperature (e.g., Minnis et al. 1992). In the present study, we use the Wood and Bretherton (2004) method to derive the cloud-top heights after evaluating it against sounding measurements. The consistency of the seasonal variations of cloud-top height between passive and active sensors gives us confidence on the sampling from the active sensors, which are then used to derive cloud-base altitude and other properties.

The purpose of this paper is to use satellite measurements that have extensive spatial and temporal coverage over the oceans to investigate the seasonal variation of the structure of MBL clouds. The paper is organized as follows: First, a brief description is given for the datasets used in our analysis. In section 3, the climatological seasonal difference between December–February (DJF) and June–August (JJA) in low cloud amount and cloud water path from the International Satellite Cloud Climatology Project (ISCCP) is first shown. Variations of cloud-top height or MBL depth using three independent sources are then presented. Cloud base and cloud physical thickness are described next, along with variations of the lifting condensation level (LCL) of near-surface air and subscale variability of cloud properties. Section 4 discusses the physical mechanism of the seasonal variation in the MBL structure and clouds. The final section contains a summary of the paper.

2. Description of data

We use the ISCCP data to describe the basic seasonal variation of MBL cloud amount and cloud water path. The long-term (1984–2004) cloud data are from the ISCCP D2 product (Rossow et al. 1996; Rossow and Schiffer 1999). The data are monthly averaged at equal area grid cell of 280-km resolution. Because the variations of both cloud amount and cloud water path will be investigated in tandem, and cloud water path is derived via visible channel, the monthly average of daytime-only data is used. The random overlap assumption is used between low-top and high-top clouds to derive a virtually unbiased low cloud amount for all months. The liquid water path of low-top clouds is derived as weighted average of all three low-top cloud types in the D2 dataset.

Cloud-top temperatures are from the Clouds and the Earth's Radiant Energy System–Moderate Resolution Imaging Spectroradiometer (CERES–MODIS) daily cloud information from Flight Model instruments FM1 and FM4 onboard satellites *Terra* and *Aqua*, respectively, for the year 2004. The data are aggregated on $1^\circ \times 1^\circ$ from original footprint data (Loeb and Schuster 2008). From the cloud-top temperature, the cloud-top height is derived using the diagnostic formula from Wood and Bretherton (2004), which was derived based on mixing-line theory making use of satellite cloud information including cloud-top temperature, low cloud amount, and cloud water path. The derived MBL depths are validated with balloon sounding data at the Atmospheric Radiation Measurement (ARM) Point Reyes Mobile Facility (further information about the deployment at Point Reyes is available online at http://www.arm.gov/sites/amf/ptreyes/).

Two other MBL depth data from spaceborne active sensors with fewer samplings are used to demonstrate the robustness of the results from the algorithm. They also serve as cross-validation for each other. One is the PBL height retrieved from the Geoscience Laser Altimeter System (GLAS) atmospheric lidar data. The other is derived from the cloud layer product of Cloud-Aerosol Lidar and Infrared Pathfinder Satellite Observations (CALIPSO).

The GLAS instrument operates from the Ice, Cloud, and Land Elevation Satellite (ICESat) and the PBL heights are derived from attenuated backscatter coefficient profiles at the 532-nm channel. PBL height is detected where there is a sharp drop in backscatter cross section because across PBL height the aerosol/cloud particle and moisture concentration generally drop dramatically. The data are available at 100-m vertical resolution and two horizontal resolutions at 1.5 km and 30 km. The lower-resolution (i.e., 30 km horizontally) PBL height can be more reliably detected and is thus used in this study. The product is generated only at nadir along the spacecraft ground track. More information for the GLAS PBL product is available in Palm et al. (2002). A brief summary of PBL height retrieval and discussion of the quality over regions of stratocumulus and trade cumulus can also be found in Ahlgrimm and Randall (2006). There are 13 ratings to describe the confidence levels of the quality of the retrieval. The rating is based on the ratio of the averaged attenuated backscatter signal within the PBL to the average signal 500 m above the PBL. It is proportional to the magnitude of the gradient of scattering at the PBL top. The larger this gradient, or equivalently the higher the particle concentration in the PBL, the easier to find the PBL top and hence the higher the confidence. Data from release 28 is used here. As in Ahlgrimm and Randall (2006), we will use all successful retrievals except PBL heights higher than 3500 m. The data starts from February 2003, but the instrument is on operational mode only for some selected periods. Therefore, only one June month and three February months are used.

The lidar instrument operating from the CALIPSO satellite, the Cloud-Aerosol Lidar with Orthogonal Polarization (CALIOP), is a two-wavelength (532 and 1064 nm) polarization-sensitive lidar that provides high-resolution vertical profiles of aerosol and clouds. The 1064-nm channel has better sensitivity in the boundary layer whereas the 532-nm channel is much more sensitive in the upper troposphere and stratosphere. The procedure for the level-2 product starts with locating the feature layers with significant signals and then uses the depolarization ratios at 532 nm to classify the features among aerosol and ice/liquid clouds. From the top down, once a cloud top is located, a ''look ahead'' strategy along with a ''probabilistic base locator'' is employed to progressively find the base. Correction of in-cloud attenuation for single or multilayer overlying clouds is considered in the process of layer locating by following the slope of the signal profiles. Virtually all boundary layer clouds are detectable at the full resolution of 30 m vertical and 333 m horizontal. More detailed documentation about CALIPSO and the algorithms can be found in Vaughan et al. (2005). The full-resolution product provides up to five cloud layers per profile. The top of the first cloud layer below 3000 m is considered the boundary layer top in our derivation. All available PBL height data within each $2.5° \times 2.5°$ grid are simply averaged to produce monthly means. Similarly, monthly means of the base of the lowest cloud layer are derived. The total physical PBL cloud thickness can be computed as the sum of the thickness of all cloud layers below 3000 m. Because of in-cloud attenuation of lidar beam, the derived cloud-base height may potentially be biased higher. The impact on the results will be discussed in section 3c.

The long-term monthly upper-air and near-surface data from the National Centers for Environmental Prediction–Department of Energy (NCEP–DOE) Second Atmospheric Model Intercomparison Project (AMIP-II) reanalysis (hereafter Reanalysis 2; Kanamitsu et al. 2002) are used to explore the influence of large-scale environment and to gauge the lower-tropospheric stability. Reanalysis 2 is based on the widely used NCEP/National Center for Atmospheric Research (NCAR) reanalysis by fixing the errors and updating the parameterizations of the physical processes. The model used for the analysis has 28 levels with T62 spectral truncation. The monthly upper-air data are produced on 17 pressure levels at $2.5° \times 2.5°$ grids.

The sea surface temperature (SST) data used in the calculation of SST advection is from the Optimum Interpolation Sea Surface Temperature Analysis version 2 (OISSTv2; Reynolds and Smith 1994; Reynolds et al.)

North American Regional Reanalysis (NARR; Mesinger et al. 2006) 3-hourly pressure-level products for year 2004 are used to assist the derivation of PBL heights from CERES–MODIS cloud-top temperatures and the follow-up estimation of actual inversion strength (IS). The NARR data are chosen because of their much higher spatial resolution. The pressure-level product has 25-hPa vertical spacing in the lower troposphere. This is in contrast with a mere four levels below 700 hPa in typical global analyses. The horizontal resolution is also much higher at 32 km. In a comparison with the Second Dynamics and Chemistry of Marine Stratocumulus field study (DYCOMS II; Stevens et al. 2003) dropsonde

measurements (results not shown), NARR analysis represents the boundary layer much better in terms of presence of inversion and its vertical location and strength than global analysis, which may miss the inversion entirely. The derivation of PBL height using the CERES cloud-top temperature and the diagnostic algorithm of Wood and Bretherton (2004) is only performed when the temperature inversion is present in the daily NARR profile because the empirical formula for the derivation is built upon a model for inversion-capped MBL.

Increasing surface latent heat flux (LHF) is considered the primary driver in MBL transition in Bretherton and Wyant (1997). Seasonal variation in latent heat flux may be important in the seasonal variation of MBL structure as well. To test it, we derive the latent heat flux from monthly surface latent heat parameter and winds from the International Comprehensive Ocean–Atmosphere Data Set (ICOADS; Worley et al. 2005; Woodruff et al. 2005). The latent heat parameter in ICOADS is defined as $(q_s - q_a)V$, where V is near-surface wind speed and $q_s - q_a$ is the near-surface air–water vapor mixing ratio saturation deficit. The actual latent heat flux is calculated by multiplying the latent heat parameter with $C_T \times L_v$, where L_v is the evaporation latent heat, and $C_T = 0.001(1 + 0.07V)$ (e.g., Wakefield and Schubert 1981) is the transfer coefficient. Near-surface air temperature and relative humidity data from ICOADS are used to compute the height of LCLs using Bolton's (1980) formula. The variation of mean LCL is used to assist the interpretation of the seasonal changes of MBL structure.

3. Results

a. Seasonal variations in cloud amount and cloud water path

Consistent with results from surface-based cloud data (Klein and Hartmann 1993), the satellite MBL cloud amount over the subtropical northeastern Pacific is maximum during the JJA season (Fig. 1a) and minimum during the DJF season (Fig. 1b). In these figures, the random overlap assumption has been used to adjust the ISCCP low-top cloud to low clouds. The random assumption takes into account the different origins of marine boundary layer clouds and middle-latitude frontal clouds. During both seasons, the peak amount is about 1000 km away from the coast. This has been presumed to result from lateral entrainment of dry/warm continental air and downstream cold surface temperature advection (e.g., Klein 1997). The wintertime subtropical peak is slightly farther away from the coast. The summertime peak is about 30% larger than that of winter.

Figures 1c,d show the mean in-cloud water path (LCWP) of low clouds for JJA and DJF, respectively. The mean values are averaged over low-top clouds only when they are not obscured by higher top clouds (i.e., no overlapping assumption is used to recover the cloud water path when the low clouds are obscured by clouds at higher altitudes). It is seen that the summertime larger cloud amount is accompanied by higher in-cloud water content. Summertime cloud water path is 50%–100% greater than that of wintertime across the domain. This is consistent with the finding in Rozendaal and Rossow (2003) that summertime Californian marine low clouds persist longer. The spatial gradient for LCWP is greater in the summer than in the winter, the same as for cloud amount. In the ISCCP product, LCWP was derived from cloud optical thickness assuming a constant effective radius of 10 μm for liquid water clouds. Retrievals from CERES–MODIS, however, have shown that the effective radius is smaller in JJA than in DJF. Therefore, the difference in LCWP between the two seasons may be overestimated in ISCCP. However, even after adjusting the monthly ISCCP cloud water path using monthly and spatially varying effective radius based on 1-yr CERES–MODIS retrievals, the LCWP is still significantly greater in summer than in winter. The LCWP from CERES–MODIS is also greater in summer than in winter (not shown).

b. Seasonal variation of MBL depth and cloud-top altitude

One fundamental MBL property is its depth. This property is expected to affect the structures of MBL clouds. In the following, we use several satellite products to illustrate the variation of MBL and the associated cloud geometric properties on a seasonal scale. The inferred change in MBL structure will be used later to explain the differences in MBL cloud physical properties between the seasons.

Figures 2a,b show the inversion base heights for the two seasons that were derived from CERES–MODIS cloud-top temperature for low clouds using the diagnostic formula of Wood and Bretherton (2004). Daily samples are included only when an inversion layer is present in corresponding NARR profile because the algorithm assumes the existence of an inversion. Results without considering the presence of an inversion layer in the NARR however are qualitatively similar because NARR almost always sees an inversion layer for most of the domain.

The most noticeable feature in the figures is that summertime MBL depth is as shallow as 500 m underneath

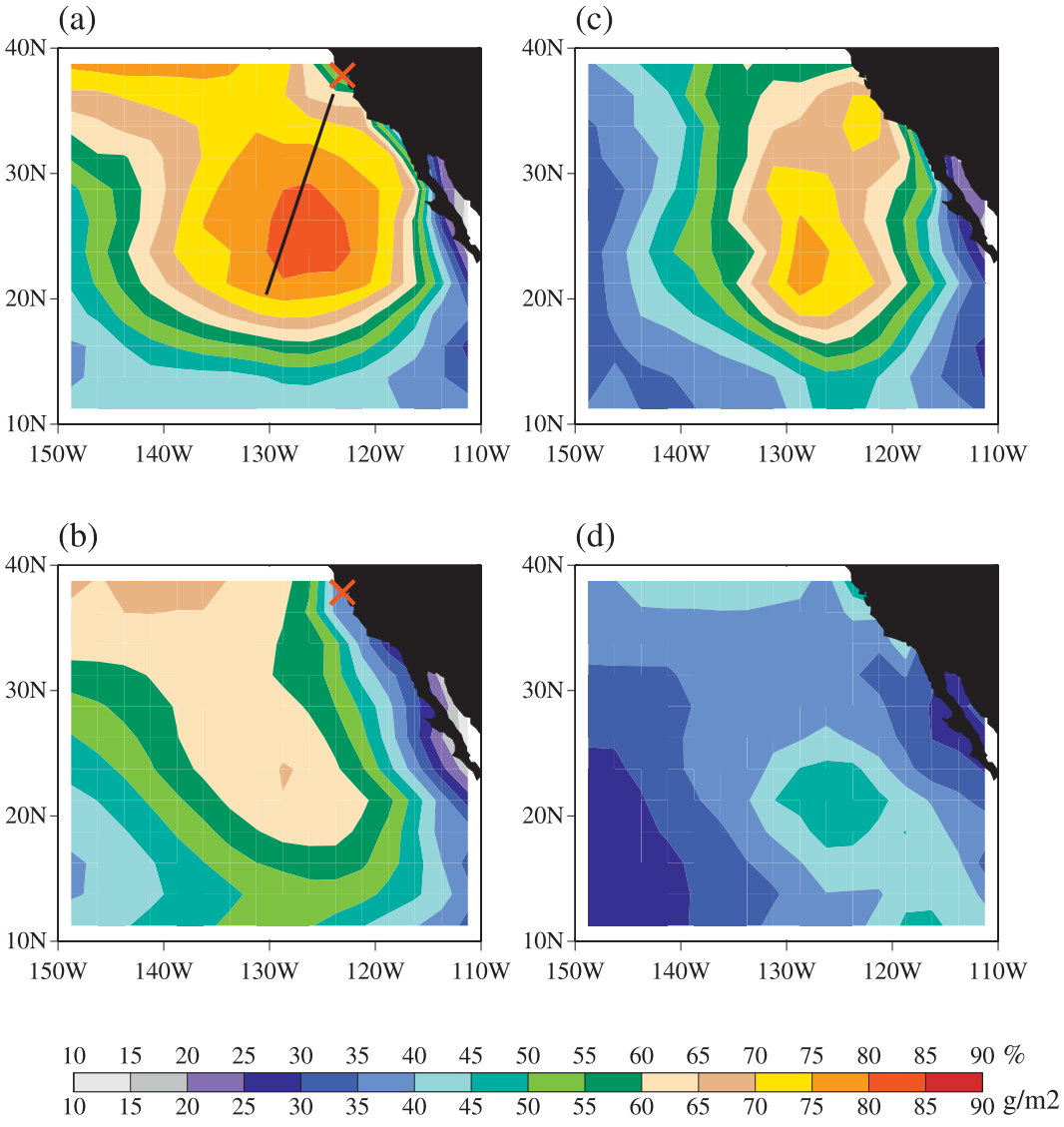

FIG. 1. (a),(b) ISCCP low cloud amount and (c),(d) in-cloud liquid water path. The upper row indicates JJA and lower row, DJF. The straight line in (a) is where the cross section is analyzed in later plots. The cross in (a) marks the location of ARM Point Reyes measurements.

the region of strongest subsidence near the coast. The inversion height generally increases westward and equatorward. The depth in summer is shallower in comparison with that in winter by more than 500 m for the entire subtropical region downstream from the coast. Although the MBL depth increases substantially downstream from the coastal region in both seasons, the seasonal difference across the region is relatively uniform.

We also used the alternative estimation of cloud-top height assuming constant lapse rate of 7.1 K km^{-1}, as in Minnis et al. (1992), for a comparison. The estimated height is about 200 m higher throughout the domain for both seasons in comparison with that in Figs. 2a,b. This difference is less than half of the seasonal difference in either estimate.

To gain further confidence on the MBL depth and its seasonality, we used high-resolution balloon soundings from the ARM mobile facility installed at Point Reyes, off the coast of San Francisco for February and July of 2005, as a validation dataset. The location is marked in red in Fig. 1a. The number of sounding profiles for February is very limited, however. Figure 3 shows the monthly mean temperature profile from the balloon soundings with the mean height from the satellite algorithm at the same location. It is clear that the satellite-

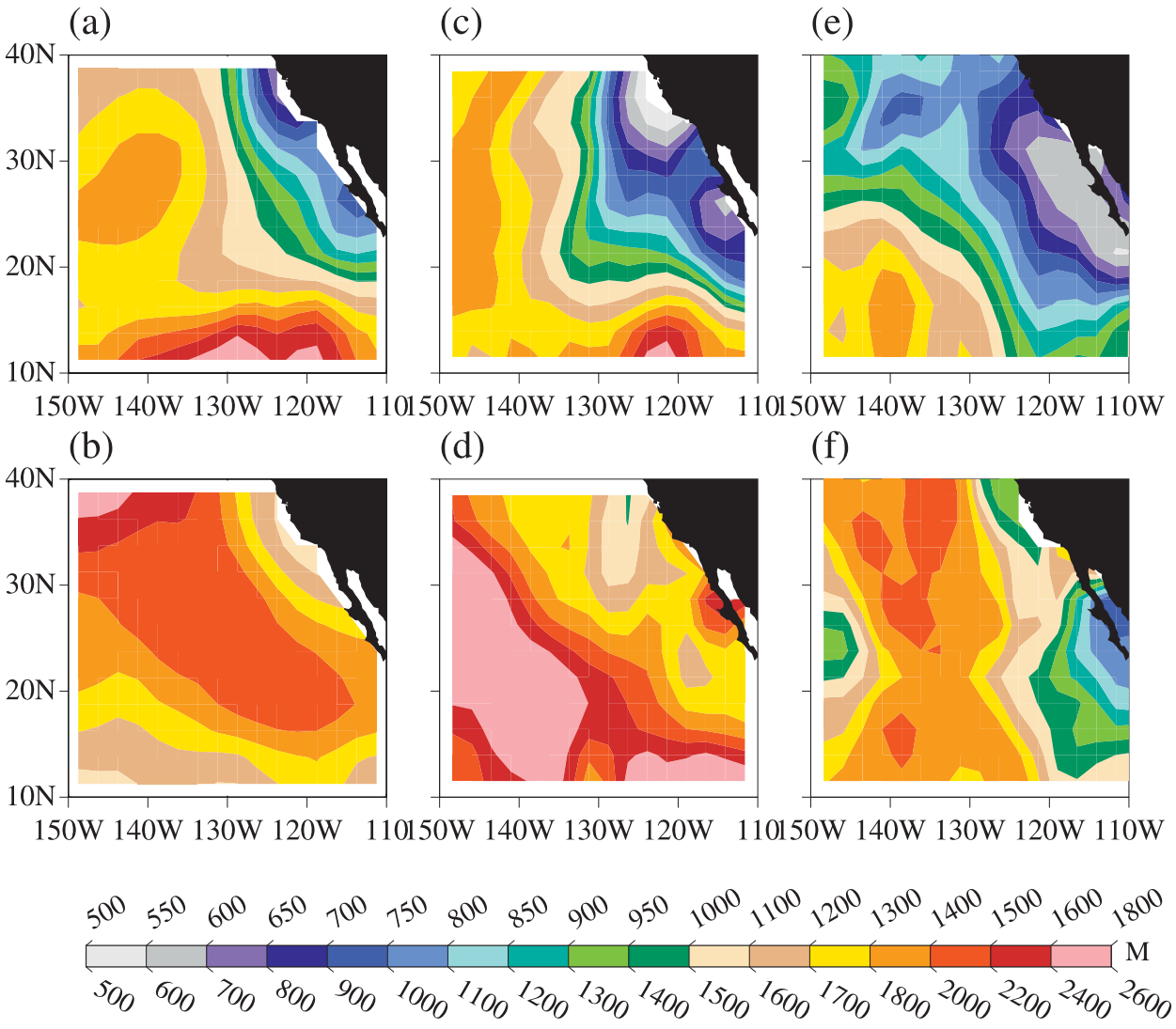

FIG. 2. Inversion heights for JJA and DJF from (a),(b) CERES, (c),(d) CALIPSO, and (e),(f) GLAS. CERES and CALIPSO use the color scale above the bar, whereas GLAS uses the color scale below the bar.

derived MBL depths are well within the range of inversion layers in the sounding data for both seasons.

More direct measurement of MBL depth from GLAS is shown in Figs. 2c,d for the months of June and February only. The temporal and spatial sampling of the GLAS product is much sparser than the CERES–MODIS product. The lidar profiling only covers two narrow slices per day over the domain. June data are available only in 2006, whereas February data are only available for 2004 through 2006. The MBL height plots are not as smooth as in Figs. 2a,b. MBL depth from GLAS is overall higher than that derived from the cloud-top temperature shown in Fig. 2a,b. Nevertheless, the shallowness of MBL near the coast in the summer and the seasonal and spatial downstream variations are robust features that are consistent with the results derived from the MODIS–CERES data.

The MBL depths from CALIPSO are shown in Figs. 2e,f for July 2006 and January 2007, respectively. The ranges of PBL heights for both seasons are comparable with that from CERES–MODIS. The seasonal variation is consistent with the results obtained from GLAS and CERES–MODIS. For example, the MBL height is about 500 m near the coast under summer conditions and more than twice as large under winter conditions. These consistencies and the validation against sounding data also suggest that cloud-top heights can be fairly accurately estimated from infrared sensors.

Among the three datasets, cloud-top altitudes from GLAS are systematically higher than those from the

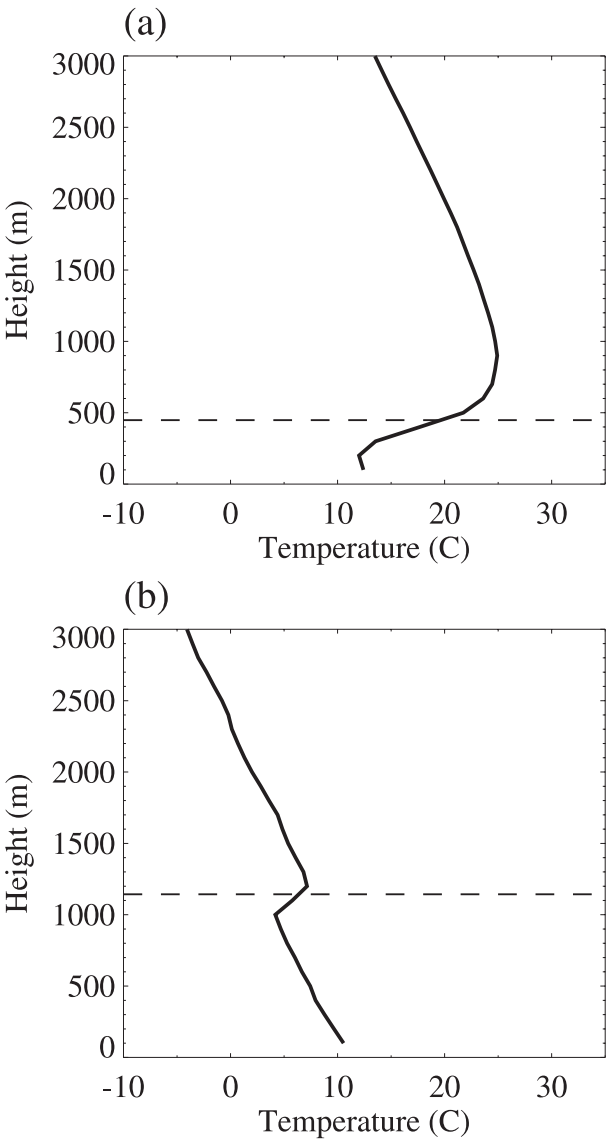

FIG. 3. ARM Mobile Facility Point Reyes mean temperature soundings for July and February 2005. The horizontal dashed lines are the collocated seasonal mean inversion base height from Figs. 2a,b.

CERES–MODIS and CALIPSO. Because GLAS and CALIPSO would detect similar cloud-top altitudes if the same cloud is measured, the difference among the datasets is very likely caused by different samplings for different months and years.

c. Seasonal variation of cloud base, LCL, MBL structure, and cloud inhomogeneity

Cloud-base height information is only available from the CALIPSO lidar measurement. This information is useful because the cloud-base height can be used to shed some light on how other low-cloud properties differ on a seasonal basis. For example, the contrast of cloud-base height with the LCL of near-surface air can offer a hint on how well the MBL is mixed and the variation between seasons.

The monthly mean cloud-base height from CALIPSO is shown in Figs. 4a,b. As expected, the cloud-base height gradually increases downstream from the coast under both summer and winter conditions. January cloud-base height is about 600 m higher than that of July. This is similar to the difference in cloud-top height. As a result, the difference in cloud physical thickness (not shown) between the seasons is small ($<$100 m). It should be noted the CALIPSO cloud-base height may be biased higher because of in-cloud attenuation of lidar beams. This, however, should not affect the sign of the seasonal variation of cloud base because, if anything, the upward bias in summer would be larger as a result of higher cloud water loading (see Figs. 1c,d). Moreover, as will be shown next, summertime cloud base and LCL of the near-surface air are very close to each other, suggesting that the bias is small because we do not expect cloud base to be lower than the LCL.

Following Miller and Albrecht (1995), we can assume that for a well-mixed MBL the averaged cloud base is close to the LCL of near-surface air. If the MBL is not well mixed, the cloud layer and subcloud layer could be decoupled. In that case, the LCL of near-surface air is still roughly coincident with the base of episodic cumulus clouds but would be below the overlying stratocumulus layer. The difference between the LCL and cloud-base height is therefore a measure of the vertical inhomogeneity of the MBL.

The climatological LCLs of near-surface air for the summer and winter seasons are shown in Figs. 4c,d, which are calculated from ICOADS near-surface climatological conditions. As expected, LCL increases with increasing distance from the coast westward and equatorward. Summertime LCLs are broadly lower than those in winter. However, the seasonal variation in LCL is much smaller than that in the cloud-base height. For summer conditions, starting from the California coast downstream to about 1000 km away, the CALIPSO cloud-base heights stay very close to the LCLs of the near-surface air. Only farther downstream, the cloud-base heights become larger than the LCLs. In contrast, the January cloud-base heights are well above the LCLs right off the coast. This clearly indicates that the summertime coastal MBL is close to well mixed whereas the wintertime MBL is decoupled starting at the upstream of the trade winds.

The larger difference between LCL and cloud-base height in the winter season also implies relatively larger presence of shallow cumulus in MBL in winter than in

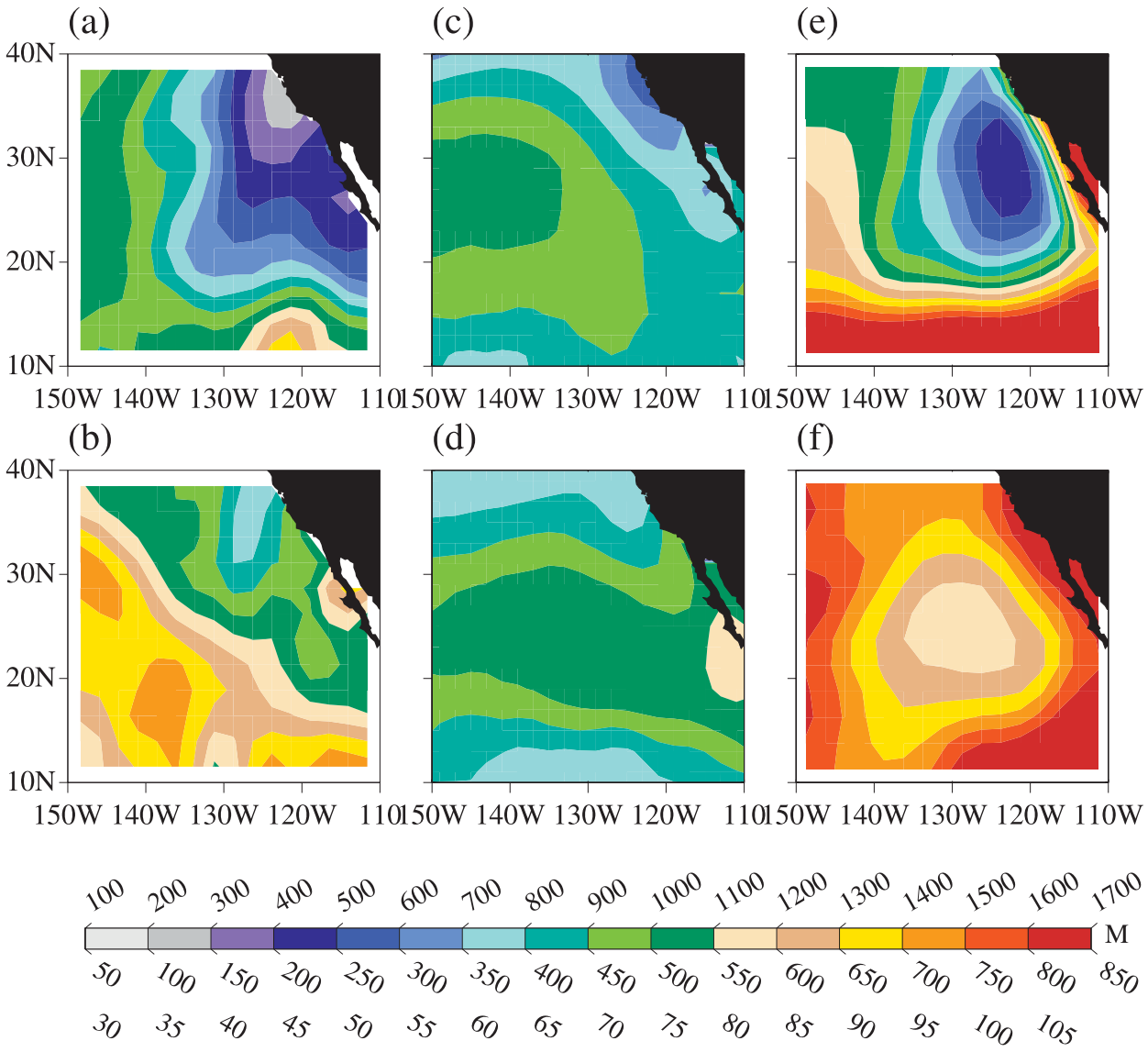

FIG. 4. (a), (b) Low-cloud base heights from CALIPSO, (c), (d) ICOADS LCL, and (e), (f) ISCCP D2 normalized spatial standard deviation of water path for (top) JJA and (bottom) DJF. The color scales from top to bottom are for cloud-base height, LCL, and normalized STD, respectively.

summer. Figures 4e,f show the spatial standard deviation of cloud water path within each ISCCP D2 equal-area cell, which is meant to represent the subgrid variabilities of clouds. The standard deviation in the figure has been normalized by the monthly mean liquid water path. Consistent with the large difference between cloud-base height and LCL, wintertime clouds have much higher subscale variability than those for the summer.

d. A summary along a cross section

We next use cloud properties for a cross section extending from the California coast to summarize the seasonal variations. The cross section is about 2000 km offshore as shown in Fig. 1a. It approximately follows the annual mean surface air trajectories. Figure 5a shows that the amount of low clouds increases from the winter (dashed) to the summer (solid), and from the coast to the open ocean in both seasons. The magnitude of this seasonal variation is rather uniform and it is approximately equal to the spatial variation along the cross section. Figure 5b shows that the in-cloud liquid water path in the summer is over 50% more than that in the winter.

Figures 5c,d show the cloud-top and cloud-base heights, respectively. For cloud-top height, only those derived from CERES–MODIS and CALIPSO are shown. The CERES–MODIS data are given in thin solid

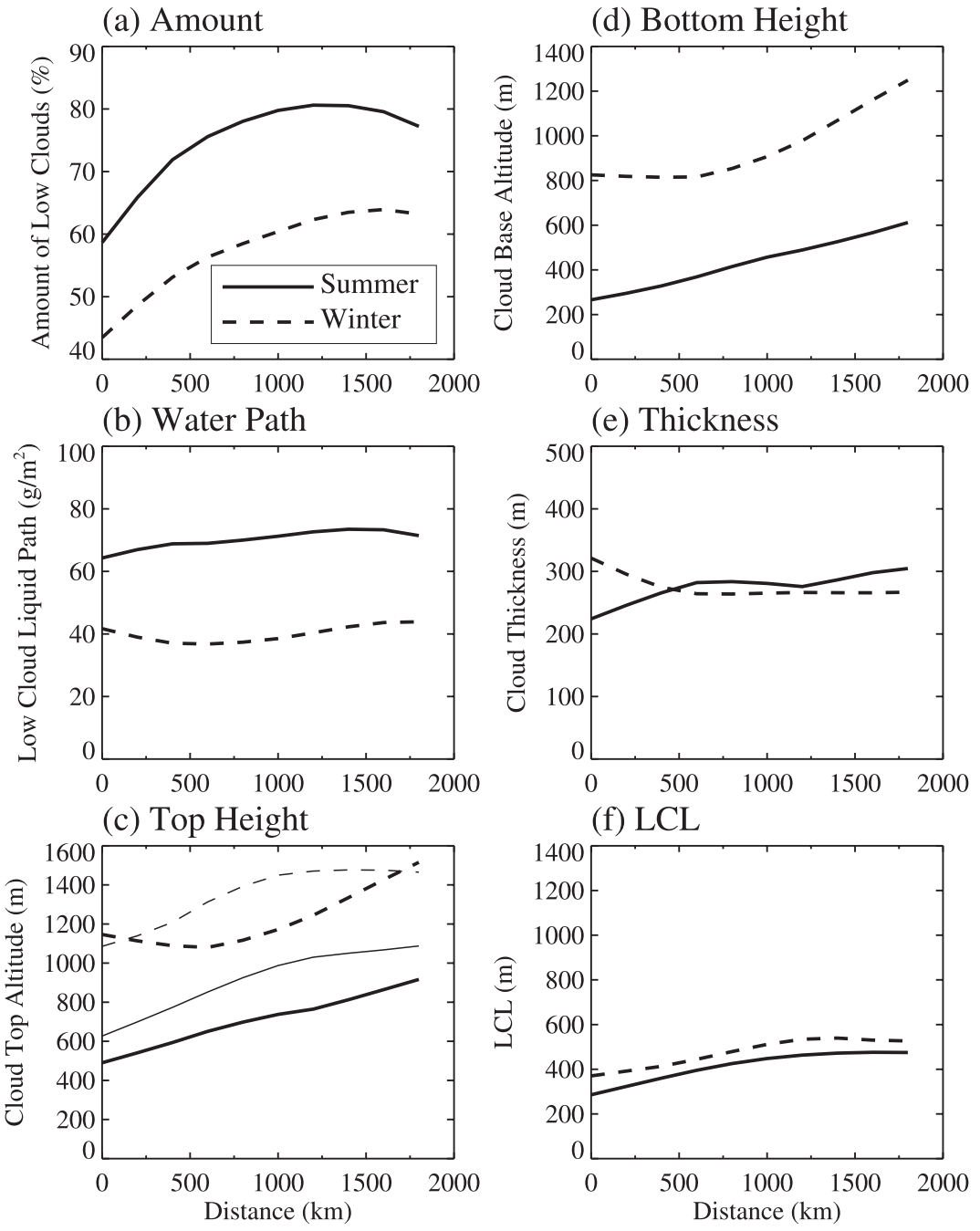

FIG. 5. Cloud properties along the cross section in Fig. 1a starting off the California coast to the open ocean. The solid line indicates summer and the dashed line, winter. For cloud-top height, the thick lines are from CALIPSO and the thin lines are from CERES–MODIS.

(summer) and thin dashed (winter) lines; the CALIPSO data are given in thick lines. It is seen that relative to the winter, summer clouds have lower tops and bases. Although cloud properties vary a lot along the cross section, their seasonal variation is much more uniform. Figure 5c also shows that the seasonal variation of cloud-top height is a robust feature even though the height values differ between CERES–MODIS and CALIPSO as a result of different samplings and uncertainties in the algorithms.

The physical thickness of clouds along the cross section is shown in Fig. 5e. They are remarkably similar

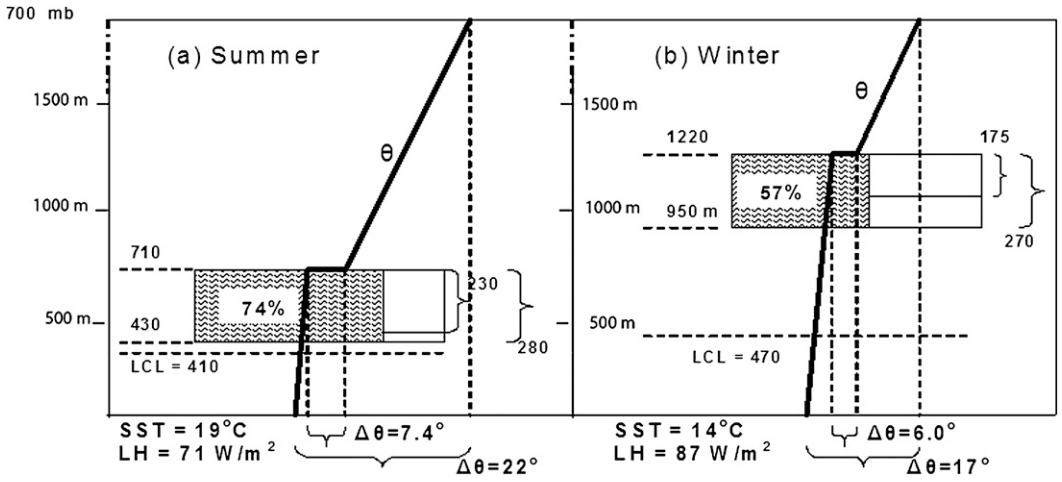

FIG. 6. Schematics of the seasonal contrast of low clouds between (a) summer and (b) winter. The numbers represent averages along the cross section in Fig. 1a. Shown are the cloud amount (in percentage) in the shaded box, cloud-top and cloud-base heights as well as LCL to the left of the shaded box, and cloud thickness and adiabatic liquid water thickness to the right of the cloud box. The adiabatic liquid water thickness is calculated from the in-cloud liquid path. The thick lines represent schematic vertical profiles of potential temperature. Shown at the bottom are SST, LHF, LTS, and IS.

between the seasons and along the cross section, between 200 and 300 m. Because they represent monthly averages, the thickness of the stratocumulus must be even less when cumulus clouds are present. Cloud thickness increases slightly from the coast to the open ocean in the summer but decreases in the winter. The shallowness of these clouds makes it a daunting task to simulate them in coarse-resolution models.

The LCLs along the cross section for the two seasons are shown in Fig. 5f. The seasonal difference is small, with LCL in the winter slightly higher. The LCLs are close to the cloud-base height in the summer but much lower than the cloud-base height in the winter.

The above results are summarized schematically in Fig. 6. The numbers in the figure represent the averages along the cross section used in Fig. 5. The adiabatic cloud thickness is derived by using the LCWP assuming an adiabatic distribution of cloud liquid water within clouds.

4. Discussion of the mechanism

Monthly MBL cloud amount has been shown to correlate well with the LTS (Klein and Hartmann 1993). Traditionally, LTS is defined as the potential temperature difference of air at 700 hPa and at the surface. The JJA and DJF LTS during the period of 1984–2004 from NCEP Reanalysis 2 are shown in Figs. 7a,b. In addition to the downstream decrease of LTS, the seasonal variation is very significant throughout the domain.

LTS consists of stratifications of three sections in the lower troposphere (e.g., Wood and Bretherton 2006), including the actual inversion strength and the cumulative stratifications below and above the inversion layer. The free-troposphere portion is proportional to the product of the depth of the dry atmosphere layer below 700 mb and its lapse rate, which is considered close to moist adiabat. The MBL portion below inversion can be straightforwardly calculated given surface and cloud-top temperatures. Therefore, with the assumption of a thin inversion layer, once the height of an inversion layer is known, the inversion strength can be indirectly estimated by subtracting the other two stratifications from LTS. Uncertainties in the procedures are not expected to affect much of the seasonal results. Figures 6c,d show the inversion strength using daily CERES–MODIS cloud-top temperatures and NARR analysis. It is seen that the summertime larger LTS also occurs with stronger inversion strength. The seasonal variation of the LTS, however, consists of a significant fraction from the free-troposphere stratifications (not shown) because of the large change in inversion height and increased moist adiabatic lapse rate of potential temperature with temperature in the summer. Given the same surface temperature and LTS, lower cloud top would correspond to weaker MBL inversion. In the summer, MBL is lower but LTS is larger as a result of larger seasonal variation of the free-tropospheric temperature than that of the SST. These two effects compensate each other, leading to a much smaller seasonal variation of the inversion strength relative to that of the LTS. Wood and Bretherton (2006) pointed out that the relationship between LTS and inversion strength may

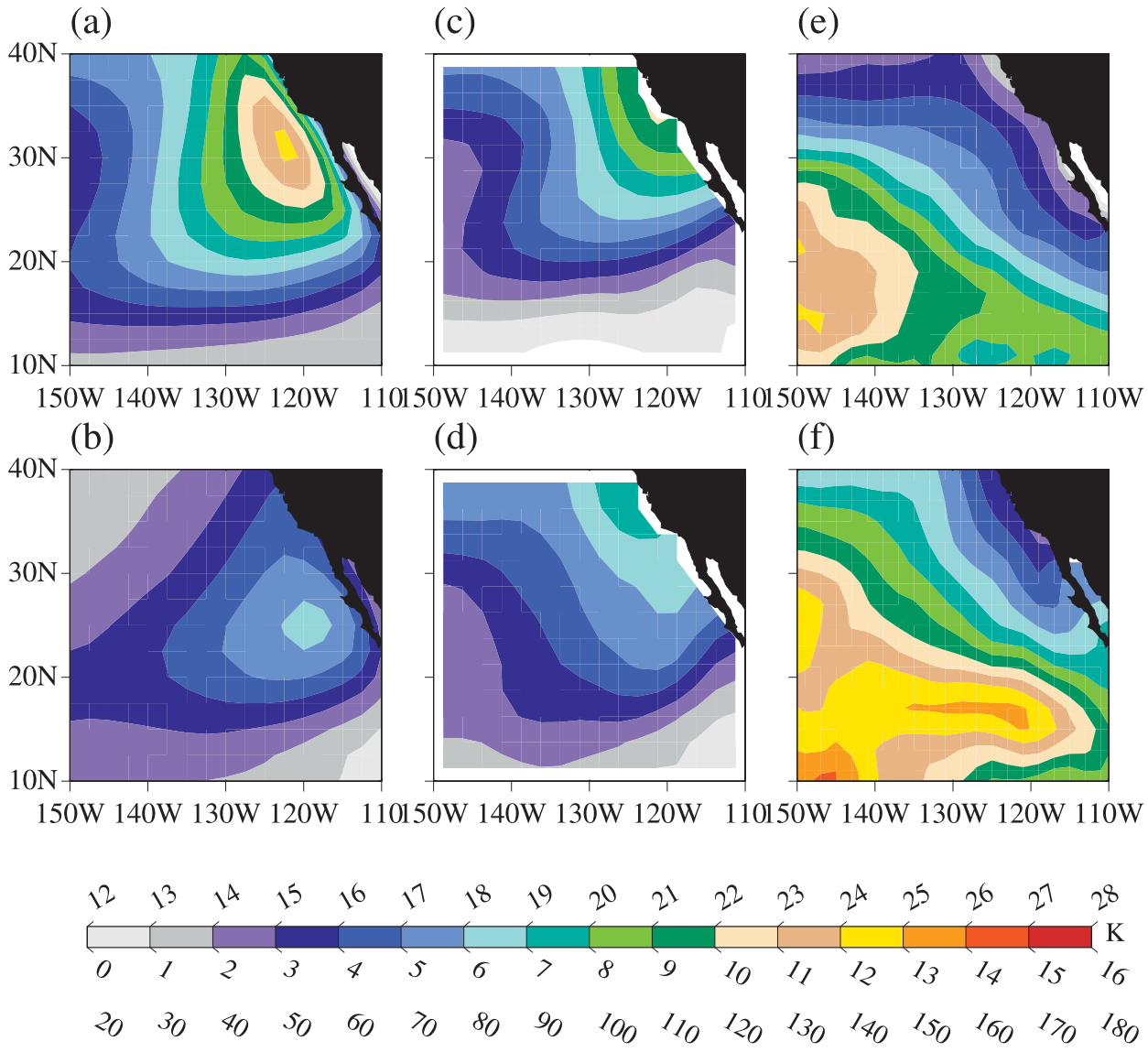

FIG. 7. (a),(b) LTS from NCEP Reanalysis 2, (c),(d) IS from CERES, and (e),(f) surface LHF from ICOADS. The upper row indicates JJA and the lower row, DJF. The color scales from top to bottom are for LTS, IS, and LHF (in W m^{-2}), respectively.

not be valid when the free-tropospheric temperature has a significant seasonal cycle. Our analysis shows that this relationship is significantly weakened on seasonal scale because of seasonal variation of the inversion height.

The LTS and inversion strength along the cross section in Fig. 1a are shown in Figs. 8a,b. The LTS in the summer peaks about 500 km off the coast. It varies little in the winter along the cross section. At any location, the LTS in the summer is larger than that in the winter. This, however, is not the case for inversion strength. The inversion strengths decrease more from the coast to the open ocean than from summer to winter.

What then causes the seasonal variation of the observed changes of low clouds and their heights? The inversion layer is formed where the turbulent PBL air meets the subsiding warm air. In a scenario in which MBL cloud has yet to form and so turbulences driven from MBL top can be neglected, the surface-driven turbulence is the primary force to overcome the descending motion. Descending air with larger LTS (summer) tends to create a larger convective inhibition for the surface-based turbulent updrafts. Therefore, for a given strength of surface-based updraft, the penetration depth of the updrafts is shallower. This would set a stage of a lower inversion base and shallower MBL in

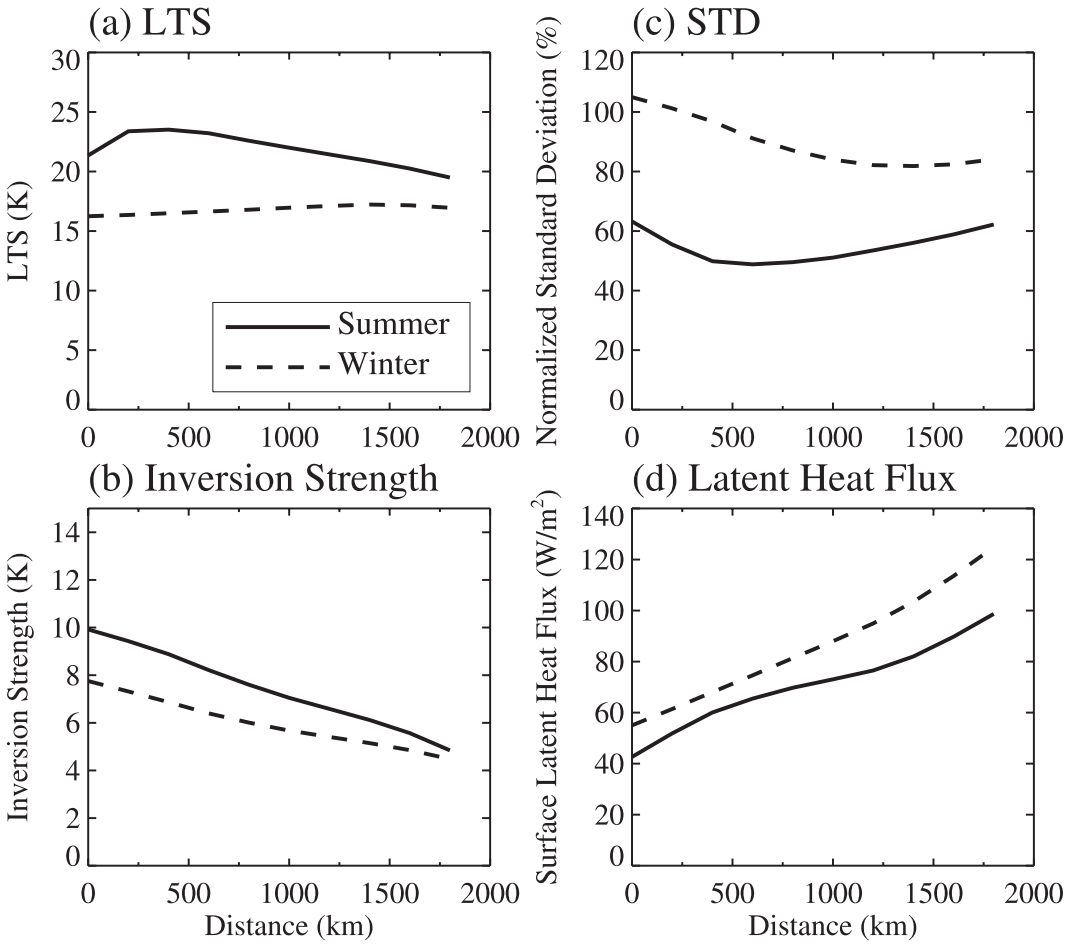

FIG. 8. Large-scale meteorological conditions, normalized standard deviation of in-cloud liquid water, and surface LHF along the cross section in Fig. 1a starting off the California coast to the open ocean. The solid line indicates summer and the dashed line, winter.

which moisture is trapped and cloud is formed. Lower inversion base height favors creation of weaker inversion strength as noted previously, but the effect of larger LTS dominates. The net effect is the stronger inversion strength, which also acts to limit the entrainment deepening at the cloud top after cloud is formed. The resulting shallower MBL would be better mixed, favoring stratiform clouds. This is consistent with the case for the summer MBL off California that has higher cloud amount with smaller inhomogeneity compared to that associated with the deeper MBL in the wintertime.

Cloud-top entrainment has a positive feedback to the seasonal variation of low clouds caused by the initial inversion strength. Higher wintertime entrainment dilution is initially caused by the weaker inversion strength. This can lead to more efficient entrainment of dry air from above, enhancing surface latent heat flux. Figures 7e,f compare the surface latent heat fluxes between the two seasons. The enhanced latent heat flux in the winter favors the decoupling of MBL (Bretherton and Wyant 1997). The distribution of cloud inhomogeneity and latent heat flux along the cross section are shown in Figs. 8c,d.

The above characterization of the seasonal variation of low clouds from summer to winter shares many features of the spatial variation of clouds from the coast to the open ocean. These include cloud amount, in-cloud liquid content, cloud-top and cloud-base heights, and spatial inhomogeneities within clouds. For the spatial variation, Bretherton and Wyant (1997) described an MBL deepening–warming decoupling mechanism to explain the stratocumulus-to-cumulus transition. They showed that decoupling of the MBL occurs when the ratio of cloud-top cooling rate to surface latent heat flux falls below the minimum decoupling threshold. Along the surface air trajectories over study domain, surface latent heat fluxes increase because of higher SSTs, which lead the stratocumulus to break.

In the seasonal variation of clouds, surface latent heat flux appears to be a result, not the cause, of the decoupling. In the summer, clouds are confined lower than those in winter; latent heat flux is smaller because of the smaller moisture deficit of surface air relative to the ocean. Once the seasonal contrast of surface flux is created, Bretherton and Wyant's (1997) mechanism can be used to explain the other aspects of the cloud seasonal variations. According to Bretherton and Wyant (1997), for typical summer MBL, decoupling requires a surface latent heat flux close to 100 W m^{-2}. As shown before, the latent heat flux in the summer is well below 100 W m^{-2} as far as 1000 km away from the coast. This can probably explain why the coastal MBL is very close to well mixed in summer. In winter, the cloud-top radiative cooling is smaller, as is the requirement for surface latent heat flux to meet the decoupling criterion. Calculations using the NCAR Community Atmosphere Model (CAM) column radiation model and typical January versus July surface and atmospheric conditions show that the cloud-top radiative cooling rate for each of the ISCCP low-cloud bins is at least 30% smaller in winter than in summer, even when the clouds are placed at the same height for both seasons. As a result, as shown in Fig. 7f, although the wintertime surface latent heat flux along the cross section is not substantially larger than that in summer, it is sufficient for the ratio of the cooling rate to fall below the decoupling threshold. This can explain why wintertime MBL is fully decoupled starting right off the coast.

Although the seasonal variation of surface latent heat flux is not simply caused by the change of SST, one can consider it to be because of the warming of SST relative to the air temperature of the free troposphere. In this context, the Bretherton and Wyant (1997) deepening–warming mechanism can be directly used to explain the seasonal variation of low clouds.

The schematic vertical distribution of potential temperature, the LTS, and the inversion strength for the two seasons are shown in Fig. 6. The numbers represent averages along the cross section defined before. Relative to the potential temperature at 700 mb, the SST warms by 5°C from summer to winter, even though the actual SST decreases by 5°C, from 19° to 14°C.

There may be other factors responsible for causing the observed seasonal changes of low clouds. These include the magnitude of surface temperature, the rate of large-scale subsidence, and the horizontal temperature advection near the surface (Klein 1997). In the summer, SST over the study region is about 2°C warmer, the subtropical high is stronger, and the rate of subsidence is slightly stronger and spatially more uniform than in the winter. But sorted by horizontal temperature advection at the surface and 850-hPa pressure vertical velocity, the seasonal contrast of low clouds remains the same for the same advection and subsidence rate bins as shown in Fig. 9. We also sorted low clouds by using SST and subsidence. The same results are obtained (figure not shown). We therefore conclude that the relative change of surface temperature to the free-tropospheric air temperature is at least one of the dominant controls of the seasonal variation of low clouds.

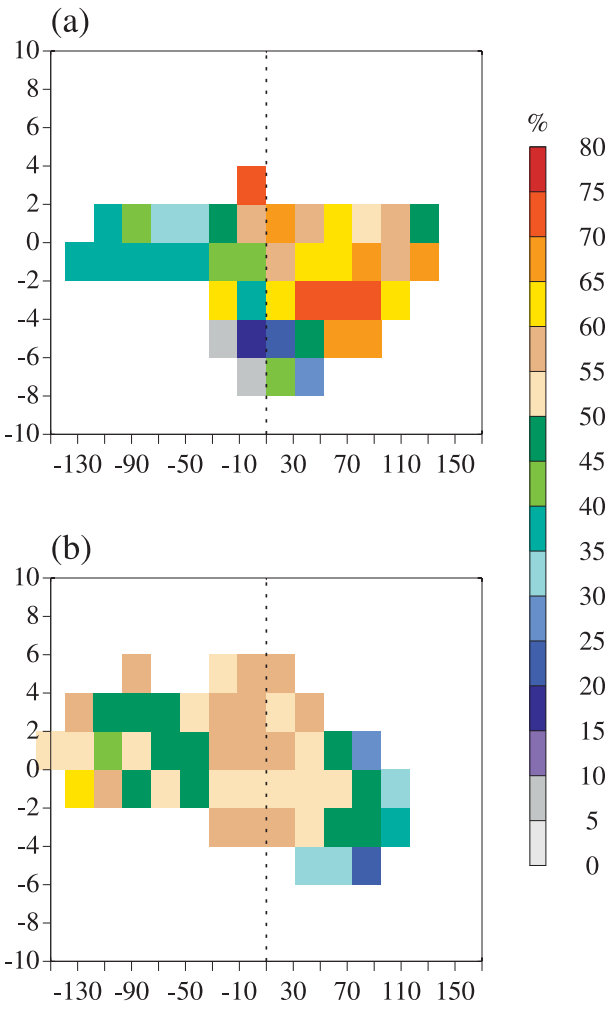

FIG. 9. ISCCP low clouds sorted by SST advection (ordinate in K day^{-1}) and 850-hPa subsidence rate (abscissa in hPa day^{-1}) for (a) summer and (b) winter.

5. Summary

ISCCP cloud data and three other special satellite retrievals have been used to characterize the seasonal variations of MBL clouds off California and the associated MBL structures. New results are summarized as follows:

- In addition to larger amount of low clouds in summer than in winter off the California coast (as shown in

previous investigations), summertime MBL clouds also contain more in-cloud condensed water.
- The top and base altitudes of MBL clouds are lower in the summer than in the winter.
- MBL cloud base is approximately the same as the LCL of the near-surface air in the summer, but it is much higher than LCL in the winter. The MBL is better mixed in the summer, with horizontally more homogeneous stratiform clouds.
- The surface latent heat flux is smaller in the summer as a result of a shallower and better-mixed MBL than in the winter.
- The MBL inversion strength is larger in the summer than in the winter. This is primarily governed by the much larger seasonal variation of free-tropospheric temperature than that at the surface. There is a strong negative feedback from the MBL depth to the seasonal variation of the inversion strength. The cloud properties, in particular cloud types and cloud water path, are therefore only weakly constrained by the LTS.
- The characteristics of the seasonal variation of low clouds from summer to winter are similar to the stratocumulus-to-cumulus transition. They can be explained by using the MBL deepening–warming mechanism described in Bretherton and Wyant (1997), except that the warming of SST is relative to the free-tropospheric air temperature, which occurs in the winter.

Considering the difficulties in modeling low clouds in climate models and the lack of physical understanding of MBL clouds (e.g., Zhang et al. 2005; Bony and Dufresne 2005), the results presented in this paper should provide a useful observational basis for the validation of GCM simulation of MBL clouds and the associated MBL structures.

Acknowledgments. We wish to thank the two anonymous reviewers whose comments have led to important improvements of the original manuscript. The authors would like to acknowledge that GLAS data are obtained from NSIDC, CALIPSO data from NASA Langley ASDC, NARR data from NOMADS, and ICOADS data from the NOAA/OAR/ESRL PSD. This research is supported by the NASA MAP program and the DOE ARM program to the Stony Brook University.

REFERENCES

Ahlgrimm, M., and D. A. Randall, 2006: Diagnosing monthly mean boundary layer properties from reanalysis data using a bulk boundary layer model. *J. Atmos. Sci.,* **63,** 998–1012.

Albrecht, B. A., D. A. Randall, and S. Nicholls, 1988: Observations of marine stratocumulus clouds during FIRE. *Bull. Amer. Meteor. Soc.,* **69,** 618–626.

——, C. S. Bretherton, D. Johnson, W. H. Schubert, and A. S. Frisch, The Atlantic Stratocumulus Transition Experiment—ASTEX. *Bull. Amer. Meteor. Soc.,* **76,** 889–904.

Bolton, D., 1980: The computation of equivalent potential temperature. *Mon. Wea. Rev.,* **108,** 1046–1053.

Bony, S., and J.-L. Dufresne, 2005: Marine boundary layer clouds at the heart of tropical cloud feedback uncertainties in climate models. *Geophys. Res. Lett.,* **32,** L20806, doi:10.1029/2005GL023851.

Bretherton, C. S., and M. C. Wyant, 1997: Moisture transport, lower-tropospheric stability, and decoupling of cloud-topped boundary layers. *J. Atmos. Sci.,* **54,** 148–167.

——, and Coauthors, 2004: The EPIC 2001 stratocumulus study. *Bull. Amer. Meteor. Soc.,* **85,** 967–977.

Kanamitsu, M., W. Ebisuzaki, J. Woollen, S.-K. Yang, J. J. Hnilo, M. Fiorino, and G. L. Potter, 2002: NCEP–DOE AMIP-II Reanalysis (R-2). *Bull. Amer. Meteor. Soc.,* **83,** 1631–1643.

Klein, S. A., 1997: Synoptic variability of low-cloud properties and meteorological parameters in the subtropical trade wind boundary layer. *J. Climate,* **10,** 2018–2039.

——, and D. L. Hartmann, 1993: The seasonal cycle of low stratiform clouds. *J. Climate,* **6,** 1587–1606.

Krueger, S. K., G. T. McLean, and Q. Fu, 1995: Numerical simulations of the stratus-to-cumulus transition in the subtropical marine boundary layer. Part I: Boundary-layer structure. *J. Atmos. Sci.,* **52,** 2839–2850.

Lilly, D. K., 1968: Models of cloud-topped mixed layers under a strong inversion. *Quart. J. Roy. Meteor. Soc.,* **94,** 292–309.

Loeb, N. G., and G. L. Schuster, 2008: An observational study of the relationship between cloud, aerosol and meteorology in broken low-level cloud conditions. *J. Geophys. Res.,* **113,** D14214, doi:10.1029/2007JD009763.

Menzel, W., R. Frey, B. Baum, and H. Zhang, 2006: Cloud top properties and cloud phase algorithm theoretical basis document, version 7. University of Wisconsin—Madison SSEC Publication 06.10.M2, 55 pp. [Available online at http://modis-atmos.gsfc.nasa.gov/_docs/MOD06CT:MOD06CT_ATBD_C005.pdf.]

Mesinger, F., and Coauthors, 2006: North American Regional Reanalysis. *Bull. Amer. Meteor. Soc.,* **87,** 343–360.

Miller, M. A., and B. A. Albrecht, 1995: Surface-based observations of mesoscale cumulus–stratocumulus interaction during ASTEX. *J. Atmos. Sci.,* **52,** 2809–2826.

Minnis, P., P. W. Heck, D. F. Young, C. W. Fairall, and J. B. Snider, 1992: Stratocumulus cloud properties derived from simultaneous satellite and island-based instrumentation during FIRE. *J. Appl. Meteor.,* **31,** 317–339.

Nicholls, S., 1984: The dynamics of stratocumulus: Aircraft observations and comparisons with a mixed layer model. *Quart. J. Roy. Meteor. Soc.,* **110,** 783–820.

Palm, S., W. Hart, D. Hlavka, E. J. Welton, A. Mahesh, and J. Spinhirne, 2002: GLAS atmospheric data products. Geoscience Laser Altimeter System algorithm theoretical basis document, version 4.2, 137 pp.

Randall, D. A., 1980: Conditional instability of the first kind upside-down. *J. Atmos. Sci.,* **37,** 125–130.

——, and Coauthors, 2007: Climate models and their evaluation. *Climate Change 2007: The Physical Science Basis,* S. Solomon et al., Eds., Cambridge University Press, 589–662.

Reynolds, R. W., and T. M. Smith, 1994: Improved global sea surface temperature analyses. *J. Climate,* **7,** 929–948.

——, N. A. Rayner, T. M. Smith, D. C. Stokes, and W. Wang, 2002: An improved in situ and satellite SST analysis for climate. *J. Climate,* **15,** 1609–1625.

Rossow, W. B., and R. A. Schiffer, 1999: Advances in understanding clouds from ISCCP. *Bull. Amer. Meteor. Soc.,* **80,** 2261–2287.

——, A. W. Walker, D. E. Beuschel, and M. D. Roiter, 1996: International Satellite Cloud Climatology Project (ISCCP) documentation of new cloud datasets. World Meteorological Organization Tech. Doc. WMO/TD 737, 115 pp.

Rozendaal, M. A., and W. B. Rossow, 2003: Characterizing some of the influences of the general circulation on subtropical marine boundary layer clouds. *J. Atmos. Sci.,* **60,** 711–728.

Stevens, D., and Coauthors, 2003: Dynamics and Chemistry of Marine Stratocumulus—DYCOMS-II. *Bull. Amer. Meteor. Soc.,* **84,** 579–593.

Turton, J. D., and S. Nicholls, 1987: Diurnal variation of stratocumulus. *Quart. J. Roy. Meteor. Soc.,* **113,** 969–1009.

Vaughan, M. A., D. M. Winker, and K. A. Powell, 2005: Part 2: Feature detection and layer properties algorithms. CALIOP Algorithm Theoretical Basis Document CALIPSO PC-SCI-202, Release 1.01, 87 pp.

Wakefield, J. S., and W. H. Schubert, 1981: Mixed-layer model simulation of eastern North Pacific stratocumulus. *Mon. Wea. Rev.,* **109,** 1952–1968.

Wood, R., and C. S. Bretherton, 2004: Boundary layer depth, entrainment, and decoupling in the cloud-capped subtropical and tropical marine boundary layer. *J. Climate,* **17,** 3576–3588.

——, and ——, 2006: On the relationship between stratiform low cloud cover and lower-tropospheric stability. *J. Climate,* **19,** 6425–6432.

Woodruff, S. D., H. F. Diaz, S. J. Worley, R. W. Reynolds, and S. J. Lubker, 2005: Early ship observational data and ICOADS. *Climatic Change,* **73,** 169–194.

Worley, S. J., S. D. Woodruff, R. W. Reynolds, S. J. Lubker, and N. Lott, 2005: ICOADS release 2.1 data and products. *Int. J. Climatol.,* **25,** 823–842, doi:10.1002/joc.1166.

Zhang, M. H., and Coauthors, 2005: Comparing clouds and their seasonal variations in 10 atmospheric general circulation models with satellite measurements. *J. Geophys. Res.,* **110,** D15S02, doi:10.1029/2004JD005021.